Electronic structure and thermoelectric properties: $PbBi_2Te_4$ and related intergrowth compounds

Lijun Zhang and David J. Singh
Materials Science and Technology Division, Oak Ridge National Laboratory, Oak Ridge, Tennessee 37831-6114, USA
(Received 22 April 2010; revised manuscript received 2 June 2010; published 17 June 2010)

The layered $PbTe:Bi_2Te_3$ intergrowth compound, $PbBi_2Te_4$, and related materials are investigated using first-principles calculations and Boltzmann transport theory. The electronic structures of these compounds are closely related to those of the end points, especially Bi_2Te_3 but the band gaps are larger than those of Bi_2Te_3. The calculated thermopowers are comparable to those of Bi_2Te_3 at similar doping levels but extend to higher temperatures due to the larger band gaps with the implication that the thermoelectric performance of these compounds will be best at temperatures above the range of Bi_2Te_3.

DOI: 10.1103/PhysRevB.81.245119 PACS number(s): 72.20.Pa, 72.15.Jf

I. INTRODUCTION

Thermoelectrics provide a useful solid-state technology for power generation and refrigeration. The efficiency of thermoelectric devices is limited by a material-dependent figure of merit $ZT=\sigma S^2T/\kappa$, where T is the absolute temperature, σ and κ are the electrical and thermal conductivities, and S is the thermopower. Currently used materials have $ZT\sim 1$ or lower. This limits the efficiency of thermoelectric power generation to a few percent. Finding practical materials with higher performance is challenging because the transport coefficients entering ZT have opposite dependencies on materials parameters. For example, S generally increases as the doping level is reduced, but this leads to lower σ. Similarly, introduction of scattering by disorder, for example, can lower the lattice thermal conductivity κ_l, but at the same time this normally lowers the mobility and thus σ.[1–3]

The most widely used thermoelectric materials for near-room-temperature (up to 200 °C) applications are doped semiconductor alloys based on $(Bi,Sb)_2Te_3$, with peak ZT values of 0.8–1.1.[2,4] In fact, extrapolation of the below-room-temperature thermoelectric properties of Bi_2Te_3 to higher T would predict excellent properties in the important temperature range from 100 °C to 400 °C. This is, however, not realized because the actual performance falls off due to bipolar conduction. This is a result of the small band gap of Bi_2Te_3, $E_g\sim 0.13$ eV.[5–7] This limits the applications of Bi_2Te_3, and consequently materials such as PbTe with ZT of $\sim$0.8 are preferred for power generation above 200 °C.[2] There have been recent developments that greatly improve the performance of PbTe-based thermoelectrics,[8,9] but nonetheless a Bi_2Te_3-like thermoelectric with better high-temperature performance would be very desirable. In this regard it should be mentioned that the performance of Bi_2Te_3-based thermoelectrics can be substantially improved via nanostructuring, as was shown in alloys with Sb_2Te_3 where high values of $ZT=1.4$ were achieved in nanostructured bulk samples.[10]

Here, we study members of the quasibinary $(A^{IV}B^{VI})_m(A_2^VB_3^{VI})_n$ systems, where $A^{IV}=Ge,Sn,Pb$; $A^V=Sb,Bi$; and $B^{VI}=Se,Te$,[11–19] with emphasis on $PbBi_2Te_4$. These materials usually occur with tetradymite (Bi_2Te_2S)-type layered structures and may be regarded as intergrowths of PbTe-type (rocksalt) and Bi_2Te_3-type (hexagonal) phases. This is illustrated for $(PbTe)_1(Bi_2Te_3)_1$, namely, $PbBi_2Te_4$, in Fig. 1. There are experimental results that suggest that there are good thermoelectric materials in this family. As might be expected from more complex structures relative to Bi_2Te_3-based solid solutions, very low thermal conductivity κ ($\sim$1 W/m K) was reported.[14,20] A high power factor $\sigma S^2=14\times10^{-4}$ W/m K^2 at 600 K was found in samples of the $PbTe:Bi_2Te_3$ system[11,16] and in particular values of ZT as high as 0.5 were found in $(PbTe)_1(Bi_2Te_3)_2$, i.e., $PbBi_4Te_7$.[14,16] At least some of these compounds ($PbBi_4Te_7$) are reported to be congruently melting.[17] Band-gap values of 0.19–0.22 eV were reported for the related compounds $Ge(Sn)Bi_2Te_4$ and $Ge(Sn)Bi_4Te_7$.[11,15] These values, which are larger than those of Bi_2Te_3 even though the same Bi_2Te_3 layers are present in the structure, suggest the possibility that they may be Bi_2Te_3-like materials but with higher operating temperatures. Key questions are the extent to which ZT can be improved through optimization of the carrier concentration in these materials and to what extent the analogy with Bi_2Te_3 holds.

Here, we investigated electronic structures and thermoelectric properties for the first class (single layer) of materi-

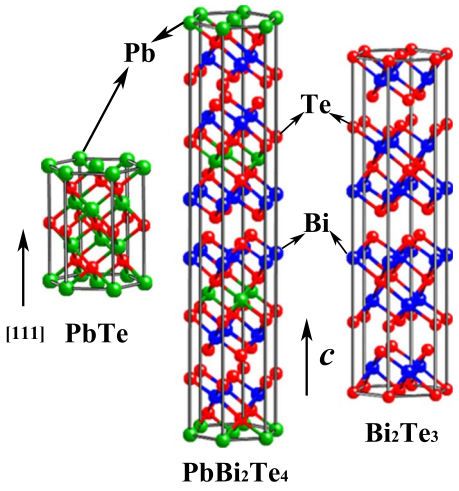

FIG. 1. (Color online) Crystal structure of the first compound in the quasibinary PbTe-Bi_2Te_3 system; $PbBi_2Te_4$ (middle) shown in the hexagonal unit cell, as compared to PbTe (left) and Bi_2Te_3 (right). For the rocksalt-type PbTe, the cell is oriented along the [111] direction.

als, specifically, $PbBi_2Te_4$, $PbBi_2Se_4$, and $SnSb_2Te_4$, based on density-functional calculations and Boltzmann transport theory.

II. COMPUTATIONAL METHODS

The electronic structure calculations were performed using the general potential linearized augmented plane-wave (LAPW) method,[21] with the augmented plane-wave plus local orbitals (APW+lo) implementation[22] in the WIEN2K code.[23] We used two exchange-correlation potentials. These were the commonly used generalized gradient approximation (GGA) of Perdew, Burke, and Ernzerhof (PBE-GGA),[24] and the Engel-Vosko GGA (EV-GGA).[25] Standard GGA functionals are based on the expression for the total energy in terms of the coupling constant averaged exchange-correlation hole and are designed to reproduce the total energy as well as possible.[26] The Engel-Vosko functional was designed to reproduce the true exchange-correlation potential instead. As such, it gives improved band gaps at the expense of a poor description of the total energy. Here, we use the PBE-GGA for structural properties and the EV-GGA for transport calculations because the improved band gap is important for the thermopower and other transport quantities especially at higher temperatures (see below).

Spin-orbit interactions are potentially important for compounds containing heavy p elements, such as Pb and Bi, and in fact this is the case for PbTe and Bi_2Te_3. Therefore, we included spin-orbit in the calculations. This was done using a second variational procedure. In addition to band states, we included relativistic $p_{1/2}$ local orbitals[21] in the spin-orbit calculation. These were found to be useful in accurately determining the electronic structure of Bi_2Te_3.[27,28] We used LAPW spheres of radii $2.5a_0$ for Pb and Bi; $2.3a_0$ for Sn, Sb, and Te; and $2.1a_0$ for Se, with well-converged basis sets determined by $R_{\min}k_{\max}=8.0$, where $R_{\min}$ is the minimum LAPW radius and $k_{\max}$ is the plane-wave cutoff. The Brillouin-zone (BZ) samplings were checked by directly increasing the density of the **k**-point meshes until convergence was reached, that is, until the changes in calculated properties were insignificant. The thermopower at low T and low carrier concentration was the most sensitive quantity to the zone sampling. When underconverged calculations were done the results showed deviations from the expected Mott behavior, i.e., the expectation that the thermopower should linearly approach zero at 0 K was violated in that case. This observation was helpful in checking that the calculations were converged. For all materials the experimental lattice constants were used while the internal atomic coordinates were optimized by total-energy minimization based on the PBE-GGA.

Transport functions, particularly the temperature- and doping-dependent thermopower, $S(T)$, were calculated from the first-principles electronic structures using Boltzmann transport theory[29,30] with the constant scattering time approximation (CSTA). The needed integrations were done with the BOLTZTRAP code.[31] As mentioned, transport properties can be very sensitive to the BZ sampling particularly for low doping levels and low temperatures. We calculated the electronic structures to be used in the transport calculations using very dense meshes up to $32\times32\times32$ in the rhombohedral BZ. The BOLTZTRAP code uses an analytical Fourier interpolation of the band structure. This interpolation is used to produce a finer mesh for the integrations over the Brillouin zone. Furthermore, because this interpolation is based on smooth analytical functions, the velocities needed can be calculated directly as $\nabla_{\mathbf{k}}\varepsilon$, where ε are the band energies. This is described in detail in Ref. 31. Also, as mentioned, the band gap can be important for the transport properties, especially at high temperatures where bipolar conduction can occur. For Bi_2Te_3 the calculated band gap with the PBE-GGA is 0.082 eV while the band gap with the EV-GGA is 0.127 eV. The latter value is in good agreement with the experimental value of $\sim$0.13 eV.[5,6] Finally, we note that we use carrier concentration as the fundamental variable in discussing the transport properties. In practice, the calculations were done as a function of Fermi energy, using the band structures for the stoichiometric compound. This amounts to treating the doping as a rigid band shift. In this regard, we note that doping can in principle modify the shape of the band edges depending on the details of the doping method and carrier concentration. We neglect such effects. Since the density of states (DOS) is nonconstant, the carrier concentration at fixed Fermi energy is a function of temperature. This function was computed and its inverse was then used to obtain the transport quantities as functions of carrier concentration from the results as functions of Fermi energy.

III. CRYSTAL STRUCTURE

As shown in Fig. 1, the unit cell of $PbBi_2Te_4$ may be described as Bi_2Te_3-like and PbTe-like layers stacked along the c-axis direction and separated by van der Waals gaps.[32] The space group is $R\bar{3}m$.[11,18] These structures are closely related to that of Bi_2Te_3. As in Bi_2Te_3, the layers may be regarded as composed of Te intercalated with metal atoms. Within the layers the bonding is qualitatively similar to that of rocksalt-type PbTe (see the left panel of Fig. 1), where each atom is octahedrally coordinated by six nearest neighbors, except that there are short and long bonds between Bi and Te as might be expected. The extra layers in $PbBi_2Te_4$ with respect to Bi_2Te_3 lead to a larger c lattice parameter, 41.677 Å,[11] as compared with 30.440 Å.[33] This type of crystal structure suggests a tendency to form stacking faults, so that samples with substantial disorder in the sequence of Bi_2Te_3 and PbTe layers may be made. It will be of interest to study the effect of this on transport, especially the thermal conductivity.

In our calculations we used the experimental lattice parameters, $a=4.439$ Å and $c=41.677$ Å for $PbBi_2Te_4$,[11] and fully optimized the internal atomic positions. The resulting bond lengths are 3.22 Å for Pb-Te, and 3.08 and 3.25 Å for the two inequivalent Bi-Te distances. These are in good accord with the experimental values of 3.16 Å for Pb-Te, and 3.08 and 3.33 Å for Bi-Te.[18] We followed a similar procedure and obtained a similar level of agreement for isostructural $PbBi_2Se_4$ and $SnSb_2Te_4$. In particular, for $PbBi_2Se_4$ we obtain a Pb-Se bond length of 3.02 Å, as compared to the

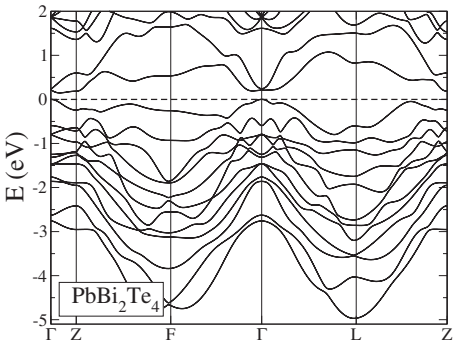

FIG. 2. Electronic band structure of $PbBi_2Te_4$ calculated using the EV-GGA along the high-symmetry lines in the rhombohedral Brillouin zone. The valence-band edge is set as energy zero and denoted with a dashed line.

reported value of 3.04 Å. The calculated Bi-Se bond lengths are 2.86 and 3.07 Å, as compared to the experimental values of 2.97 and 3.04 Å. In $SnSb_2Te_4$ we obtain a Sn-Te bond length of 3.14 Å vs the experimental value of 3.09 Å, while the calculated Sb-Te bond lengths are 3.01 and 3.18 Å, in comparison with 2.99 and 3.20 Å.[18,19]

IV. $PbBi_2Te_4$: ELECTRONIC STRUCTURE

We begin with $PbBi_2Te_4$. The calculated EV-GGA band structure and the corresponding electronic DOS for $PbBi_2Te_4$ are shown in Figs. 2 and 3. Figure 4 is a comparison of the band structure in a scalar relativistic approximation with that including spin-orbit. The effect of spin-orbit is significant as reflected, for example, in the size of the band gap. We emphasize that all the transport calculations below employed the band structure with spin-orbit.

As may be seen, we obtain a narrow-gap semiconductor with an indirect band gap of 0.148 eV. This is ~0.02 eV larger than Bi_2Te_3. The valence-band maximum is located at the Γ point and the conduction-band minimum is along the Γ-Z direction. Relatively flat bands appear in the Γ-Z direction as expected from the layered structure. Both the valence and conduction bands have mixed character derived from Pb-Te (for clarity, Te states are not shown) and Bi-Te states. This includes the bands at the band edges. The implication is that both Pb and Bi-Te layered blocks will contribute to the transport. Interestingly, there are heavy bands below the valence-band maximum. These lead to peaks in the DOS with both Pb and Bi s states at valence bands ~−0.5 eV relative to the band edge. PbSe and PbTe also show band structures with heavy bands below the band edge, which have lighter mass near the valence-band maximum. In those materials these heavier bands contribute to an enhancement of the thermopower at elevated temperature and doping level.[34,35]

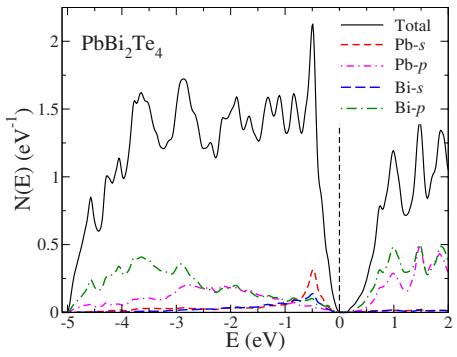

FIG. 3. (Color online) Calculated total and projected (for Pb and Bi) DOS of $PbBi_2Te_4$ with the EV-GGA. The total DOS is shown in per Te unit and projections are per atom. The projections are onto the LAPW spheres. Thus, the projected DOS are underestimated but are proportional to the atomic contributions for extended orbitals that have significant weight outside the corresponding LAPW sphere radii.

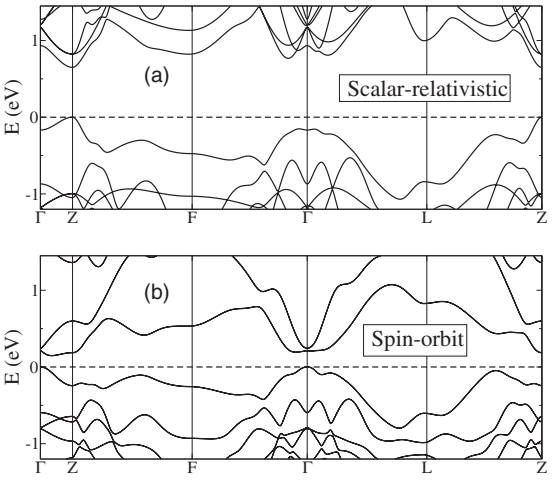

FIG. 4. Comparison of the Engel-Vosko band structure around the gap within a scalar relativistic approximation (top) and including spin-orbit (bottom).

Turning to the conduction bands, there are two low-lying bands, of which the lower one is generally heavy while the upper one is more dispersive. This combination of heavy and light bands is often favorable for a thermoelectric material since the light band favors reasonable conductivity, while the heavy band sets a low-energy scale that can enhance the thermopower.[36–38] The low-energy scale arises because for fixed carrier concentration the density of states, transport functions, and other properties are stronger functions of energy in a heavy band. For example, in the case of a single parabolic band, with effective mass m, the distance of the Fermi energy from the band edge varies as $1/m$, and so the characteristic energy scale at a given carrier concentration varies as $1/m$. Near the band edges the valence bands of $PbBi_2Te_4$ are generally heavier than the conduction bands, as is clear from the high DOS near valence-band edge. These heavy bands may be expected to contribute to high thermopower with the p-type doping, while n-type samples will need lower absolute carrier concentrations to achieve similar thermopowers. Both the valence and conduction bands are substantially nonparabolic on the energy scale of 0.1 eV, which is relevant for the $S(T)$ at ambient temperature and above [generally bands within $\sim 5kT$ of the Fermi energy contribute significantly to $S(T)$ due to the energy factor $(\varepsilon-\mu)$ in Eq. (3); see below]. Also, it should be noted that

although both Pb and Bi states occur in the DOS the shape of the band edges is more closely related to Bi_2Te_3 than PbTe. For example, PbTe shows a strongly nonparabolic light band at the band edge that becomes heavier as the carrier concentration is increased.[39] The similarity with Bi_2Te_3 is perhaps expected since Bi_2Te_3 is a layered compound. $PbBi_2Te_4$ may therefore be regarded as a intercalated version of Bi_2Te_3. On the other hand, PbTe is a three-dimensional cubic rocksalt structure compound, and so breaking it into layers separated by Bi_2Te_3 would be expected to very strongly modify its electronic structure.

The results calculated with PBE-GGA are quite similar, except that the band gap $E_g=0.093$ eV is smaller. Therefore, for $PbBi_2Te_4$, both PBE-GGA and EV-GGA yield larger band gaps than they give for Bi_2Te_3, consistent with observed larger band gaps for this family in experiments.[11,15] This increase in the band gap is perhaps surprising at first sight since in a composite one might expect the gap to be that of the lowest gap component. However, while the electronic structure of Bi_2Te_3 is anisotropic, it is not strictly two dimensional. Therefore, the gap increase that may be viewed as a weak quantum confinement effect occurs when the Bi_2Te_3 layers are separated by the PbTe blocks, although strain effects cannot be excluded.

V. THERMOELECTRIC PROPERTIES

We performed calculations for $PbBi_2Te_4$ based on the EV-GGA electronic structures. Within Boltzmann theory the temperature- and doping-level-dependent conductivity $\sigma(T,\mu)$ and thermopower $S(T,\mu)$ are given by

$$\sigma_{\alpha\beta}(T,\mu)=\frac{1}{\Omega}\int \sigma_{\alpha\beta}(\varepsilon)\left[-\frac{\partial f_\mu(T,\varepsilon)}{\partial\varepsilon}\right]d\varepsilon, \quad (1)$$

$$S_{\alpha\beta}=\sum_\gamma (\sigma^{-1})_{\alpha\gamma}\nu_{\beta\gamma}, \quad (2)$$

with

$$\nu_{\alpha\beta}(T,\mu)=\frac{1}{eT\Omega}\int \sigma_{\alpha\beta}(\varepsilon)(\varepsilon-\mu)\left[-\frac{\partial f_\mu(T,\varepsilon)}{\partial\varepsilon}\right]d\varepsilon. \quad (3)$$

Here, ε are band energies, f_μ is the Fermi distribution function, μ is the chemical potential that is actually temperature dependent, T is the temperature, and Ω is the volume. The essential terms in all three formulas are the energy projected conductivity tensors (transport distributions),

$$\sigma_{\alpha\beta}(\varepsilon)=\frac{1}{N}\sum_{i,\mathbf{k}} \sigma_{\alpha\beta}(i,\mathbf{k})\delta(\varepsilon-\varepsilon_{i,\mathbf{k}}), \quad (4)$$

which can be expressed using $\mathbf{k}$-dependent conductivity tensor as

$$\sigma_{\alpha\beta}(i,\mathbf{k})=e^2\tau_{i,\mathbf{k}}v_\alpha(i,\mathbf{k})v_\beta(i,\mathbf{k}), \quad (5)$$

where i is the band index, $\mathbf{k}$ is the reciprocal vector, N is a normalization depending on the number of k points sampled in the BZ, $\tau_{i,\mathbf{k}}$ is a scattering time, and $v_\alpha(i,\mathbf{k})$ is the i component of band velocity $\nabla_{\mathbf{k}}\varepsilon(\mathbf{k})$.

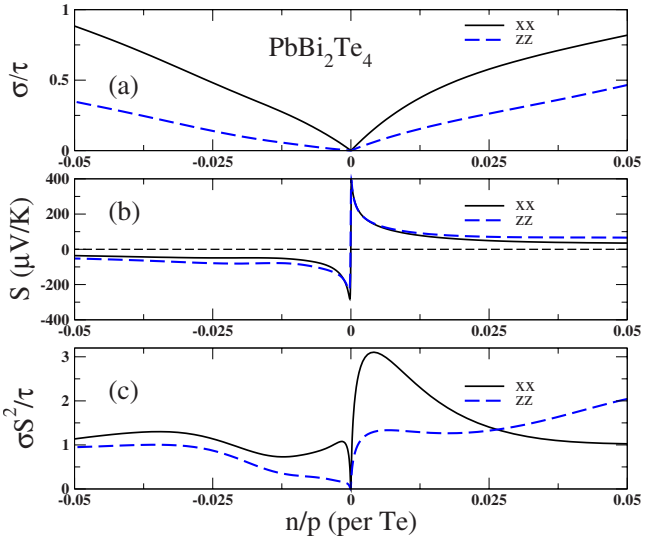

FIG. 5. (Color online) Calculated transport coefficients for in-layer, *ab*-plane (xx), cross-layer, and *c*-axis (zz) directions in $PbBi_2Te_4$, as functions of carrier concentration at 300 K: (a) electrical conductivity divided by scattering time, σ/τ; (b) thermopower; and (c) power factor divided by scattering time, $\sigma S^2/\tau$. The carrier concentration is in per Te unit while the conductivity and power factor units are arbitrary. Here, positive numbers for the doping level denote *p*-type doping.

As noted, in the above expressions only the scattering time τ is not directly determined by the band structure. In general, τ depends on temperature, doping level, and also sample details, such as defect types and concentrations. To proceed, we adopt the so-called CSTA, as is often done for degenerately doped semiconductors and metals. In this approach, the scattering time τ is assumed to be independent of energy at fixed doping level and temperature. This is supported by the fact that in most cases τ is indeed a weak function of energy on the scale of kT in the inelastic scattering regime and reasonable results are usually obtained with it,[29,40,41] including many applications to thermoelectric materials.[28,31,34–37,42–47] It should be emphasized that the CSTA does not involve any assumption about the temperature or doping level dependencies of τ, which are often strong. The advantage of CSTA is that in the expression for the thermopower [Eq. (2)] τ is exactly canceled and therefore $S(T)$ can be obtained from the band structure with no adjustable parameters.

In view of the tetradymitelike layered structure and the known anisotropy of Bi_2Te_3, we begin with the anisotropy of the transport based on the CSTA.[48] Figure 5 shows calculated results of in-layer (xx) and cross-layer (zz) transport coefficients with both *n*-type and *p*-type doping. As may be expected from the structure consisting of layered slabs separated by van der Waals gaps along the *c* axis, the in-plane electrical conductivity (σ) is more than twice larger than the value for the cross-layer direction. As shown, the anisotropy is larger for *n*-type than *p*-type doping, especially at low doping levels. In contrast to σ, the anisotropy of thermopower (S) is small. This is conventional behavior common to most doped semiconductors and metals including

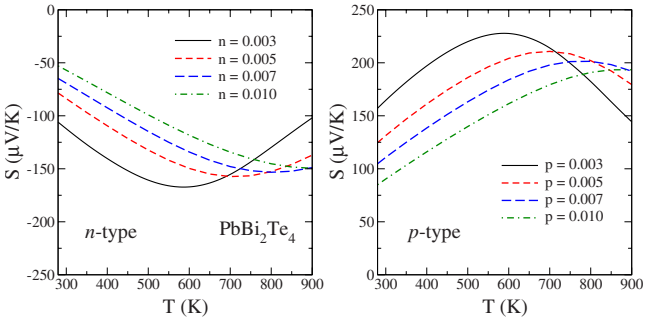

FIG. 6. (Color online) Calculated in-plane thermopower as a function of temperature for $PbBi_2Te_4$ for *n*-type (left) and *p*-type (right) doping. The doping levels are given in carriers per Te unit.

highly anisotropic materials, although there can be exceptions.[49] It arises because of the fact that $S(T)$ is a ratio in which the absolute scale of the conductivity cancels. This is the same feature that underlies the use of the CSTA to calculate $S(T)$, although we emphasize that the CSTA does not necessarily yield an isotropic thermopower for nonparabolic band structures.

Therefore, the highest power factor σS^2 will be for the in-plane direction with most of the anisotropy coming from the anisotropy of σ. Assuming that the cross-plane thermal conductivity is lower than the in-plane value, as is typically the case for layered structures, this anisotropy of the power factor will be at least partly canceled by the thermal conductivity, so that ZT will be less anisotropic. Nonetheless, it may be expected that the higher thermoelectric performance will be in the in-plane direction. This is analogous to Bi_2Te_3. In the following we focus on the in-plane $S(T)$ (note that this quantity is only weakly anisotropic).

The calculated in-plane $S(T)$ for $PbBi_2Te_4$ is given in Fig. 6 for *n*-type and *p*-type doping levels. Calculated results for Bi_2Te_3 using the same approach are shown in Fig. 7 for comparison. High thermopower is essential for high ZT. This is seen by noting that the thermal conductivity κ can generally be written as a sum of electronic and lattice contributions, κ_e and κ_l, respectively, and that κ_e is connected to electrical conductivity (σ) by the Wiedemann-Franz relation, $\kappa_e = L_0 \sigma T$, which leads to $ZT = (S^2/L_0)/(1+\kappa_l/\kappa_e)$. Therefore, for $ZT=1$, the value of thermopower S should be at least ~ 157 μV/K, assuming that the Wiedemann-Franz relation

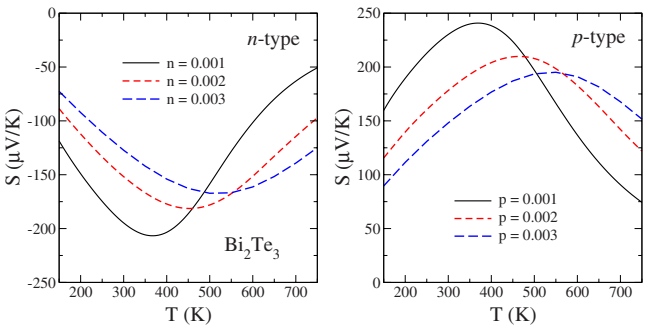

FIG. 7. (Color online) Calculated in-plane thermopower as a function of temperature for Bi_2Te_3. The doping levels are in carriers per Te unit.

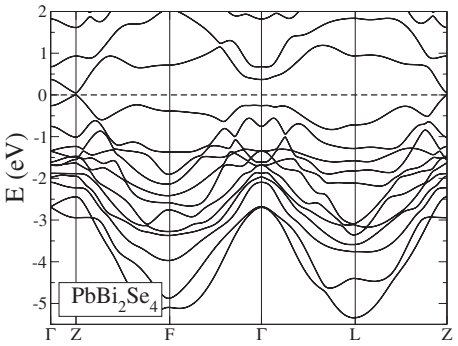

FIG. 8. Calculated band structure of $PbBi_2Se_4$ with the EV-GGA along the high-symmetry lines in the rhombohedral Brillouin zone.

with the standard value of the Lorentz number L_0 holds. This is generally the case in normal metals and degenerately doped semiconductors at ordinary temperatures. Higher thermopowers are needed if the lattice thermal conductivity is significant on the scale set by the electronic thermal conductivity. It can be seen from the calculated variation of $S(T)$ that Bi_2Te_3 is indeed a near-room-temperature thermoelectric material. This is because for doping levels where sufficiently high $S(T)$ occurs the maximum value is between 300 and 400 K, after which the thermopower falls quickly due to bipolar conduction (see also Ref. 27). While the maximum can be shifted to higher T by increasing the carrier concentration, the peak values decrease so that high ZT cannot occur based on the above considerations.

Turning to $PbBi_2Te_4$ a shift to higher T is evident particularly for *p*-type compositions, which as in Bi_2Te_3 have higher thermopowers than *n*-type at the same absolute carrier concentration. For *p*-type doping there is a range of carrier concentrations near 0.003 carriers per Te for which $S(T) > 200$ μV/K at 600 K, and high thermopowers exist up to doping levels of almost 0.01 carriers per Te. Determining the optimum doping level will depend on experimental data since it will depend on the doping-dependent balance between the electrical and thermal conductivities in this compound. This difference from Bi_2Te_3 arises from the changes in electronic structure, in particular the heavier bands and the opening of the gap, which may be due to weak quantum confinement. Thus, $PbBi_2Te_4$ and probably this family ($Pb_nBi_{2m}Te_{n+3m}$) in general are materials that with optimiza-

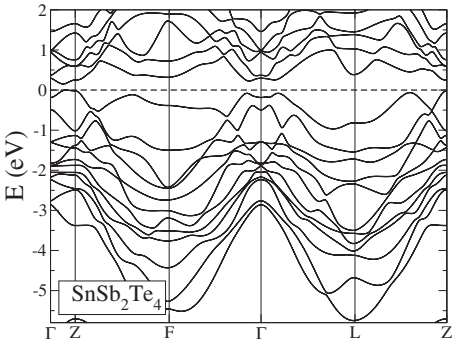

FIG. 9. Calculated band structure of $SnSb_2Te_4$ with the EV-GGA.

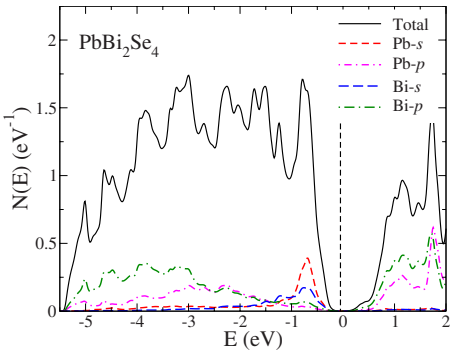

FIG. 10. (Color online) Calculated electronic DOS and projections for $PbBi_2Se_4$ using the EV-GGA. The valence-band edge is set as energy zero and denoted with a dashed line. The total DOS is shown in per Se unit and projections are per atom.

tion have promise for thermoelectric applications in the midtemperature range that is important for applications such as waste heat recovery.

VI. $PbBi_2Se_4$ AND $SnSb_2Te_4$

As mentioned, closely related compounds can be formed with the PbTe blocks replaced with SnTe or PbSe, and the Bi_2Te_3 blocks replaced with Bi_2Se_3. Thus, it is of interest to examine other compounds in this family in the context of possible development as thermoelectrics. We performed calculations as described above for the cases of $PbBi_2Te_4$, for $PbBi_2Se_4$ and $SnSb_2Te_4$. The calculated EV-GGA electronic structures including band structure and DOS for $PbBi_2Se_4$ and $SnSb_2Te_4$ are shown in Figs. 8–11. As may be seen, the general features are quite similar to those of $PbBi_2Te_4$. In particular, they are narrow-gap semiconductors, with mixed Pb-Se (Sn-Te) and Bi-Se (Sb-Te) bonding states, covalent bonding, and heavy bands near the band edges. The calculated values of band gap were 0.048 eV for $PbBi_2Se_4$ and 0.152 eV for $SnSb_2Te_4$. The smaller band gap of $PbBi_2Se_4$ is due to dispersive bands around the Z point. Interestingly, away from the gap the bands are generally heavier. As was found in PbSe,[34] this feature can extend the range for high $S(T)$ to higher T and higher carrier concentrations than would be expected in a parabolic band system with the same mass and band gap.

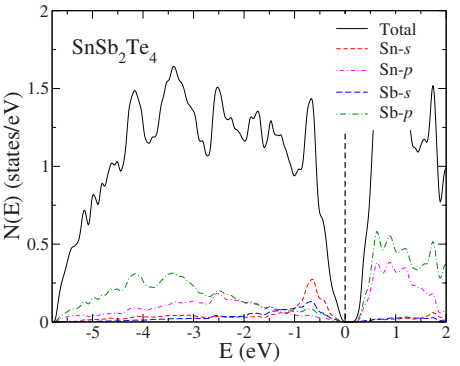

FIG. 11. (Color online) Calculated electronic DOS and projections for $SnSb_2Te_4$ using the EV-GGA.

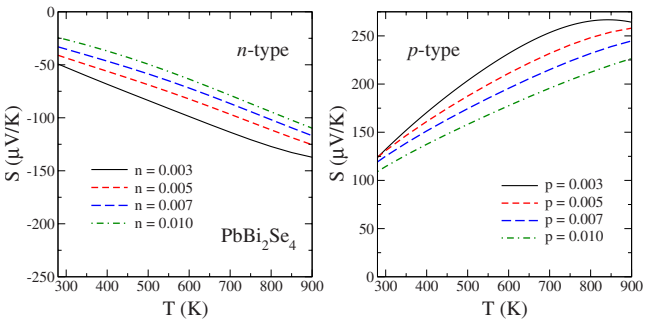

FIG. 12. (Color online) Calculated temperature dependence of in-plane thermopower at different doping levels for $PbBi_2Se_4$. The doping levels are given in carriers per Se unit.

Figures 12 and 13 show the calculated in-plane thermopowers $S(T)$ for various n-type and p-type doping levels. The results for $PbBi_2Se_4$ show close similarity with those of $PbBi_2Te_4$ (Fig. 6). In particular, high thermopowers above 160 μV/K can be obtained at temperatures as high as 550 K for p-type doping up to 0.01 holes/Se. With the n-type doping, the thermopowers are lower for comparable carrier densities. For $SnSb_2Te_4$, in addition to high thermopowers observed in higher-temperature region, the corresponding doping levels are up to 0.02 carriers/Te reflecting heavier bands.

VII. SUMMARY AND CONCLUSIONS

In summary, we have reported first-principles calculations of electronic structure and thermopower for the first members of the quasibinary systems $(PbTe)_n(Bi_2Te_3)_m$, specifically, $PbBi_2Te_4$ and related materials. Similar to Bi_2Te_3, these materials have layered structures consisting of several Te layers intercalated with metal atoms (Pb and Bi). $PbBi_2Te_4$ is a narrow-gap semiconductor, with the calculated indirect band gap of 0.148 eV, which is ~0.02 eV larger than that of Bi_2Te_3. Otherwise, the electronic structures are similar in many respects to Bi_2Te_3. The calculated thermopowers based on these show the possibility of good thermoelectric performance at temperatures above the operating range of Bi_2Te_3 reflecting the larger band gap. By comparison with Bi_2Te_3, the doping levels corresponding to similarly

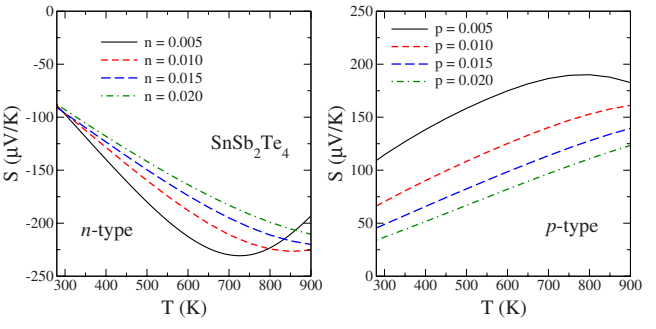

FIG. 13. (Color online) Calculated temperature dependence of in-plane thermopower at different doping levels for $SnSb_2Te_4$. The doping levels are given in carriers per Te unit.

high thermopowers are also higher (up to 0.01 carriers/Te). Similar results were obtained with $PbBi_2Se_4$ and $SnSb_2Te_4$, and for the latter the doping levels corresponding to high thermopowers for good thermoelectrics could be up to 0.02 carriers/Te. Based on the present results, it is suggested that with optimization these may be good thermoelectric materials for midtemperature applications. Finally, we note that these materials can be regarded as a very short length scale nanostructuring of Bi_2Te_3 with PbTe. It may be of interest to examine the thermoelectric properties of nanostructured Bi_2Te_3-PbTe mixtures to determine whether the quantum confinement effect discussed here and the reduction in lattice thermal conductivity that may be expected in such material would lead to an enhanced *ZT* at temperatures above those for which Bi_2Te_3 is effective.

ACKNOWLEDGMENTS

This research was sponsored by the U.S. Department of Energy, Assistant Secretary for Energy Efficiency and Renewable Energy, Office of Vehicle Technologies, as part of the Propulsion Materials Program (D.J.S.) and the S3TEC Energy Frontier Research Center (L.Z. and D.J.S.).

[1] T. M. Tritt and M. A. Subramanian, Mater. Res. Bull. **31**, 188 (2006).
[2] G. J. Snyder and E. S. Toberer, Nature Mater. **7**, 105 (2008).
[3] F. J. DiSalvo, Science **285**, 703 (1999).
[4] D. M. Rowe, *CRC Handbook of Thermoelectrics* (CRC Press, New York, 1995).
[5] R. Sehr and L. R. Testardi, J. Phys. Chem. Solids **23**, 1219 (1962).
[6] H. J. Goldsmid, *Electronic Refrigeration* (Pion, London, 1986).
[7] C. Wood, Rep. Prog. Phys. **51**, 459 (1988).
[8] F. K. Hsu, S. Loo, F. Guo, W. Chen, J. S. Dyck, C. Uher, T. Hogan, E. K. Polychroniadis, and M. G. Kanatzidis, Science **303**, 818 (2004).
[9] J. P. Heremans, V. Jovovic, E. S. Toberer, A. Saramat, K. Kurosaki, A. Charoenphakdee, S. Yamanaka, and G. J. Snyder, Science **321**, 554 (2008).
[10] B. Poudel, Q. Hao, Y. Ma, Y. Lan, A. Minnich, B. Yu, X. Yan, D. Wang, A. Muto, D. Vashaee, X. Chen, J. Liu, M. S. Dresselhaus, G. Chen, and Z. Ren, Science **320**, 634 (2008).
[11] L. A. Kuznetsova, V. L. Kuznetsov, and D. M. Rowe, J. Phys. Chem. Solids **61**, 1269 (2000), and references therein.
[12] T. Ikeda, S. M. Haile, V. A. Ravi, H. Azizgolshani, F. Gascoin, and G. J. Snyder, Acta Mater. **55**, 1227 (2007).
[13] L. E. Shelimova, O. G. Karpinskii, T. E. Svechnikova, E. S. Avilov, M. A. Kretova, and V. S. Zemskov, Inorg. Mater. **40**, 1264 (2004).
[14] L. E. Shelimova, O. G. Karpinskii, P. P. Konstantinov, E. S. Avilov, M. A. Kretova, and V. S. Semskov, Inorg. Mater. **40**, 451 (2004), and references therein.
[15] V. L. Kuznetsov, L. A. Kuznetsova, and D. M. Rowe, J. Appl. Phys. **85**, 3207 (1999).
[16] V. L. Kuznetsov, L. A. Kuznetsova, and D. M. Rowe, J. Phys. D: Appl. Phys. **34**, 700 (2001).
[17] N. S. Golovanova, V. P. Zlomanov, and O. I. Tananaeva, Inorg. Mater. **19**, 669 (1983).
[18] T. B. Zhukova and A. I. Zaslavskii, Kristallografiya **16**, 918 (1971).
[19] K. A. Agaev and S. A. Semiletov, Kristallografiya **13**, 258 (1968).
[20] L. E. Shelimova, O. G. Karpinskii, E. S. Avilov, M. A. Kretova, and C. U. Lubman, Inorg. Mater. **30**, 1412 (1994).
[21] D. J. Singh and L. Nordstrom, *Planewaves, Pseudopotentials and the LAPW Method*, 2nd ed. (Springer, Berlin, 2006).
[22] E. Sjostedt, L. Nordstrom, and D. J. Singh, Solid State Commun. **114**, 15 (2000).
[23] P. Blaha, K. Schwarz, G. K. H. Madsen, D. Kvasnicka, and J. Luitz, *WIEN2K, An Augmented Planewave Plus Local Orbitals Program for Calculating Crystal Properties* (Technische Universitat Wien, Vienna, 2002).
[24] J. P. Perdew, K. Burke, and M. Ernzerhof, Phys. Rev. Lett. **77**, 3865 (1996).
[25] E. Engel and S. H. Vosko, Phys. Rev. B **47**, 13164 (1993).
[26] J. P. Perdew, J. A. Chevary, S. H. Vosko, K. A. Jackson, M. R. Pederson, D. J. Singh, and C. Fiolhais, Phys. Rev. B **46**, 6671 (1992).
[27] P. Larson, Phys. Rev. B **68**, 155121 (2003).
[28] T. J. Scheidemantel, C. Ambrosch-Draxl, T. Thonhauser, J. V. Badding, and J. O. Sofo, Phys. Rev. B **68**, 125210 (2003).
[29] J. M. Ziman, *Principles of the Theory of Solids* (Cambridge University Press, Cambridge, England, 1972).
[30] P. B. Allen, W. E. Pickett, and H. Krakauer, Phys. Rev. B **37**, 7482 (1988).
[31] G. K. H. Madsen and D. J. Singh, Comput. Phys. Commun. **175**, 67 (2006).
[32] The crystal structure of hexagonal $PbBi_2Te_4$ as determined from x-ray diffraction has Te atoms occupying two 6*c* sites, while one 3*a* and one 6*c* cite is occupied by Pb and Bi atoms. These are difficult to distinguish using x rays alone because of the similar atomic numbers. Therefore, there is an ambiguity concerning whether these two sites are occupied by Pb/Bi atoms separately (ordered phase) or with a statistical distribution (disordered phase) (see Refs. 11, 13, 18, and 19). The first view is supported by the present calculations, e.g., the agreement between the theoretical and experimental bond lengths (see text), and is also in accord with what would be expected based on crystal chemical considerations (bond lengths, coordination, and charge states).
[33] Y. Feutelais, B. Legendre, N. Rodier, and V. Agafonov, Mater. Res. Bull. **28**, 591 (1993).
[34] L. Zhang and D. J. Singh, Phys. Rev. B **80**, 075117 (2009).
[35] D. J. Singh, Phys. Rev. B **81**, 195217 (2010).
[36] D. J. Singh and I. I. Mazin, Phys. Rev. B **56**, R1650 (1997).
[37] A. F. May, D. J. Singh, and G. J. Snyder, Phys. Rev. B **79**, 153101 (2009).
[38] L. Zhang, M. H. Du, and D. J. Singh, Phys. Rev. B **81**, 075117 (2010).
[39] D. I. Bilc, S. D. Mahanti, and M. G. Kanatzidis, Phys. Rev. B

74, 125202 (2006).
[40] W. Jones and N. H. March, *Theoretical Solid State Physics* (Wiley, London, 1973).
[41] J. B. Smith and H. Ehrenreich, Phys. Rev. B **25**, 923 (1982).
[42] D. J. Singh, *Semiconductors and Semimetals*, Thermoelectric Materials Research (Academic, New York, 2000), Vol. 70, p. 125.
[43] Y. Wang, X. Chen, T. Cui, Y. Niu, Y. Wang, M. Wang, Y. Ma, and G. Zou, Phys. Rev. B **76**, 155127 (2007).
[44] L. Lykke, B. B. Iversen, and G. K. H. Madsen, Phys. Rev. B **73**, 195121 (2006).
[45] L. Bertini and C. Gatti, J. Chem. Phys. **121**, 8983 (2004).
[46] D. J. Singh and D. Kasinathan, J. Electron. Mater. **36**, 736 (2007).
[47] G. K. H. Madsen, K. Schwarz, P. Blaha, and D. J. Singh, Phys. Rev. B **68**, 125212 (2003).
[48] Note that in the case of Bi_2Te_3 detailed comparison of the anisotropic resistivity with the anisotropy of the transport function σ/τ showed that the anisotropy of scattering time (τ) is less than 5% (see Ref. 28), while both the electrical and thermal conductivities are much more anisotropic.
[49] K. P. Ong, D. J. Singh, and P. Wu, Phys. Rev. Lett. **104**, 176601 (2010).